Functional genomics and metabolomics advance the ethnobotany of the Samoan traditional medicine "matalafi"

Seeseei Molimau-Samasoni[a,b,c,1] , Victoria Helen Woolner[b,c,d], Su'emalo Talie Foliga[e], Katharina Robichon[b,c] , Vimal Patel[b,c] , Sarah K. Andreassend[c,d] , Jeffrey P. Sheridan[b,c], Tama Te Kawa[b,c], David Gresham[f], Darach Miller[g] , Daniel J. Sinclair[h], Anne C. La Flamme[b,c,i] , Alexey V. Melnik[j], Allegra Aron[j], Pieter C. Dorrestein[j], Paul H. Atkinson[b,c,i] , Robert A. Keyzers[c,d,i] , and Andrew B. Munkacsi[b,c,i,1]

[a]Plant and Postharvest Technologies, Scientific Research Organization of Samoa, Apia, Samoa; [b]School of Biological Sciences, Victoria University of Wellington, Wellington 6012, New Zealand; [c]Centre for Biodiscovery, Victoria University of Wellington, Wellington 6012, New Zealand; [d]School of Chemical and Physical Sciences, Victoria University of Wellington, Wellington 6012, New Zealand; [e]Division of Environment and Conservation, Ministry of Natural Resources and Environment, Apia, Samoa; [f]Centre of Genomic and Systems Biology, New York University, New York, NY 10003; [g]Department of Genetics, Stanford University Palo Alto, CA 94305; [h]School of Geography, Environmental and Earth Sciences, Victoria University of Wellington, Wellington 6012, New Zealand; [i]Maurice Wilkins Centre for Molecular Biodiscovery, Victoria University of Wellington, Wellington 6012, New Zealand; and [j]Collaborative Mass Spectrometry Innovation Center, Skaggs School of Pharmacy and Pharmaceutical Sciences, University of California San Diego, La Jolla, CA 92093

The leaf homogenate of *Psychotria insularum* is widely used in Samoan traditional medicine to treat inflammation associated with fever, body aches, swellings, wounds, elephantiasis, incontinence, skin infections, vomiting, respiratory infections, and abdominal distress. However, the bioactive components and underlying mechanisms of action are unknown. We used chemical genomic analyses in the model organism *Saccharomyces cerevisiae* (baker's yeast) to identify and characterize an iron homeostasis mechanism of action in the traditional medicine as an unfractionated entity to emulate its traditional use. Bioactivity-guided fractionation of the homogenate identified two flavonol glycosides, rutin and nicotiflorin, each binding iron in an ion-dependent molecular networking metabolomics analysis. Translating results to mammalian immune cells and traditional application, the iron chelator activity of the *P. insularum* homogenate or rutin decreased proinflammatory and enhanced anti-inflammatory cytokine responses in immune cells. Together, the synergistic power of combining traditional knowledge with chemical genomics, metabolomics, and bioassay-guided fractionation provided molecular insight into a relatively understudied Samoan traditional medicine and developed methodology to advance ethnobotany.

traditional medicine | chemical biology | genomics | metabolomics | iron homeostasis

Compounds from natural resources are reliable lead templates of new pharmaceuticals, having persisted through evolutionary selection to control fundamental molecular pathways. Of the 1,562 newly approved drugs from 1981 to 2019, 64% were either natural products, derived from natural products, or based upon natural product scaffolds, biological macromolecules, or botanical drugs (1). In 2008 alone, 50% of the 255 drugs in various stages of development originated from plant natural products, demonstrating the large and yet-untapped potential of plant natural products (2).

Medicinal plants in effect have been trialed for activity through centuries of ethnobotanical use, making traditional medicines an attractive yet challenging source for further investigation (3). For example, the anti-malarial drug artemisinin was isolated from *Artemisia annua* L., a well-documented herb in traditional Chinese medicine used for the treatment of fever and malaria (4). Samoan medicinal plants also comprise such a resource, as evident by the phorbol ester prostratin, a compound sourced from the medicinal plant *Homalanthus nutans* (G.Forst) Guill., which is in development as a latency reversing agent of HIV (5–7).

Another medicinal plant commonly used in Samoa is *Psychotria insularum* A.Gray (Rubiaceae), a small tree approximately 2 m in height with small white flowers and glossy red berries. Known locally as "matalafi," the homogenate of *P. insularum* leaves (fresh leaf juice) is used to treat inflammation associated with fever, body aches, swelling, wounds, incontinence, skin infections, elephantiasis, vomiting, respiratory infections, and abdominal distress (8–12). Despite these diverse uses and wide distribution across the Pacific and in South America, the medicinal use of *P. insularum* has only been documented in the Samoan islands. Although model organisms have been used to

Significance

Medicinal plants with extensive ethnobotanical histories, particularly those from Asia, have contributed to the approval of natural compounds as pharmaceutical drugs. In contrast, Samoan traditional medicine is relatively understudied. Working with traditional healers via an ethical, data sovereignty–driven collaboration led by indigenous Samoan researchers, we elucidate the chemical biology of the poorly understood but often-used Samoan traditional medicine "matalafi," the homogenate of *Psychotria insularum* leaves commonly used to treat inflammation-associated illnesses. Our approach unifies genomics, metabolomics, analytical biochemistry, immunology, and traditional knowledge to delineate the mode of action of the traditional medicine rather than by the more common reductionist approach of first purifying the bioactive principles, which can be used to better understand the ethnobotany of traditional medicine.

validate a subset of traditional uses (10–13), the molecular mechanisms of *P. insularum* remain enigmatic. Thus far, a class of bioactive compounds common in *Psychotria* species (cyclotides) have been investigated, but these compounds have not been found in *P. insularum* (14, 15); hence the bioactive compounds mediating the biological activities of *P. insularum* remain to be identified. Here, we identified iron chelation as a mechanism of action of the *P. insularum* homogenate using chemical genomic analysis of a yeast deletion mutant library. We carried out bioassay-guided fractionation that led to the isolation and purification of rutin and nicotiflorin as bioactive constituents of the *P. insularum* homogenate, then translated our results from yeast to mammalian immune cells and validated the traditional use of the homogenate (and rutin) as an anti-inflammatory agent.

Results

Chemical Genomic Analysis Shows Metal Ion Homeostasis Is Affected by the *P. insularum* Homogenate. To understand how the *P. insularum* homogenate mediates its bioactivity, we prepared *P. insularum* leaf homogenate with a traditional healer and conducted competitive haploinsufficiency profiling genomic analysis screens for bioactivity using a pooled heterozygous deletion library of *Saccharomyces cerevisiae*. This analysis is an established method to determine mechanism of action of thousands of compounds and extracts wherein loss of mechanistically important genes results in hypersensitivity (i.e., reduced viability) (16–18). Cells were grown either in the presence or absence of 0.005% volume/volume (v/v) *P. insularum* homogenate, a concentration that reduced the growth of the pooled library by 20% compared to untreated cells. Using a false discovery rate (FDR) cutoff value of 0.025 against the chemical genomic profile of the *P. insularum* homogenate (*SI Appendix*, Fig. S1), we identified 23 gene deletions annotated with broad functions (metal ion binding, DNA binding, chromosome segregation, stress recovery, amino acid transport, vacuolar transport, transfer RNA (tRNA) methylation, and mitochondrial function) (Fig. 1*A* and *SI Appendix*, Table S1). To statistically evaluate over-representation within these 23 genes for specific molecular functions, gene ontology (GO) enrichment analysis was conducted using YeastEnrichr (19). There was significant enrichment for a multitude of processes including iron transport, DNA binding, transcription, transport of the amino acid L-aspartate, and carboxypeptidase activity (Fig. 1*B* and *SI Appendix*, Table S2). Notably, the top-ranked enrichment scores were iron ion transmembrane transporter activity (GO: 0005381) and transitional metal ion transmembrane transporter activity (GO: 0046915).

Pertinent to investigating the mechanism of *P. insularum* as a traditional medicine used by Samoan people, 9 of the 23 genes were involved in iron/zinc metabolism and are also conserved from yeast to humans (20, 21). We therefore tested whether metal supplementation would rescue the yeast growth defect in the presence of *P. insularum* by growing wild-type (WT) yeast in increasing concentrations of the homogenate alone, or with supplementation of iron ($FeCl_3$, $FeSO_4$) or zinc ($ZnCl_2$). While iron supplementation rescued the growth defect of WT in the presence of *P. insularum*, zinc supplementation did not rescue the growth defect (Fig. 1*C*). We also assessed if metal supplementation would rescue the *P. insularum*–induced growth defect of the *fet3Δ* strain, a well-characterized mutant defective in high-affinity iron uptake (22, 23). As in WT, the iron supplementation rescued the growth defect in *fet3Δ* (Fig. 1*D*), likely through low-affinity iron uptake, while zinc supplementation did not rescue the growth defect. The iron-specific rescue was not a general cytoprotective effect because supplementation with exogenous iron did not rescue generalized growth
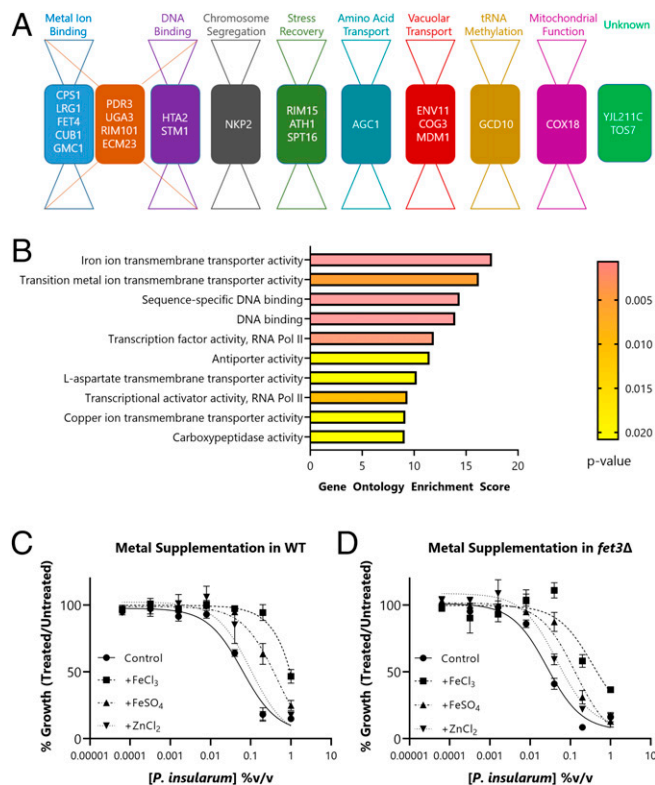

Fig. 1. Chemical genomic analysis of the *P. insularum* homogenate. (*A*) Bow-tie representation of molecular functions of the 23 genes buffering the cellular response to the *P. insularum* homogenate. The 23 genes were identified from the barcode-sequencing haploinsufficiency analysis of 6,000 heterozygous deletion strains using a statistical cutoff to detect significant differences in growth in the presence of the homogenate compared to the control (*SI Appendix*, Fig. S1). (*B*) GO enrichment analysis using YeastEnrichr distinguishes iron transport as being significantly overrepresented within the 23 genes. The enrichment score is a combined score that integrates *P* and *z*-score of expected and observed classification of a gene set to molecular functions. Percent growth of (*C*) WT or (*D*) *fet3Δ* in increasing concentrations of *P. insularum* homogenate with the absence or addition of 100 μM $FeCl_3$, $FeSO_4$, or $ZnCl_2$ compared to growth in media without *P. insularum* homogenate. Data shown are average and SD of three independent experiments, each with three technical replicates.

inhibition induced by atorvastatin (cholesterol synthesis inhibitor) or cycloheximide (protein synthesis inhibitor) (*SI Appendix*, Fig. S2). These findings directed us to an iron homeostasis mechanism of action of the *P. insularum* homogenate. Since several iron transporter deletion strains (*fet3Δ*, *ftr1Δ*, *fet4Δ*, *arn1Δ*, *arn3Δ*, *arn4Δ*, *fet5Δ*, and *fth1Δ*) involved in different aspects of iron homeostasis exhibited the hypersensitive phenotype to the *P. insularum* homogenate (*SI Appendix*, Fig. S3), it was unlikely that a single protein (24), in this case iron transporter was the physical target of the homogenate.

P. insularum Increases the Expression of Proteins Involved in Iron Transport Systems. Given that iron supplementation reduced the growth inhibitory effects of the *P. insularum* homogenate, we hypothesized that *P. insularum* homogenate was reducing intracellular iron availability, possibly via an extracellular iron-chelating mechanism. A hallmark phenotype of low intracellular iron is increased expression of iron transporter proteins (20, 21, 25). We thus monitored the expression levels of 84 proteins involved in iron transport and metabolism in the presence of the *P. insularum* homogenate or an extracellular iron chelator bathophenanthroline

disulfonic acid (BPS) relative to untreated cells. Each protein was green fluorescent protein (GFP) tagged, imaged, and quantified using confocal fluorescence microscopy relative to the constant red fluorescent protein (RFP) markers for the nucleus and cytoplasm (RedStar and mCherry, respectively) (26). Overall, the effects of the *P. insularum* homogenate were markedly similar to BPS, with identical changes in 13 proteins, of which 5 were noteworthy (Fig. 2 *A* and *B*). Relative to the untreated control, the *P. insularum* homogenate or BPS significantly increased the expression levels of the high-affinity iron transporters Fet3p-GFP and Ftr1p-GFP. The low-affinity iron transporter Fet4p-GFP also increased after treatment with the *P. insularum* homogenate or BPS, albeit less dramatically than the high-affinity iron transporters. Similarly, Arn1p-GFP (involved in the uptake of siderophore-bound iron) exhibited significantly increased abundance in the presence of the *P. insularum* homogenate when compared with the control. These transporters, together with Fet3p, Ftr1p, and

Fet4p, are known to be up-regulated under conditions of iron deprivation (20, 21, 25), further suggesting the *P. insularum* homogenate induces an iron-deficient condition. This prediction was further supported where these significant increases in protein abundance with the *P. insularum* homogenate were mirrored with growth in iron-free media, and moreover, these increased levels were restored to control levels with iron supplementation (Fig. 2 *A* and *B*).

P. insularum Reduces Intracellular Iron Content and Heme Synthesis via Iron Chelation. Our results thus far predict that the bioactive principle of the *P. insularum* homogenate reduces iron availability potentially via iron chelation. To further test this model, we measured intracellular iron levels using inductively coupled plasma mass spectrometry (ICP-MS) (27). Iron levels in lysates from untreated WT cells, or those treated with the *P. insularum* homogenate, grown in iron-free media or in the presence of BPS, were analyzed to quantify intracellular iron content. Consistent with our prediction, the *P. insularum* homogenate elicited a 60% decrease in total cellular iron in cells compared to untreated cells ($P = 0.008$) (Fig. 3*A*). Significant reductions in intracellular iron were also detected in cells grown in the BPS iron chelator control ($P = 0.008$) (60%) or cells grown in iron-free media (80%) compared to untreated cells ($P = 0.002$).

To further investigate the effect of the *P. insularum* homogenate on fundamental iron-dependent processes such as heme synthesis (28), we quantified intracellular heme using a colorimetric assay (29). The *P. insularum* homogenate conferred a significant 50% reduction ($P = 0.002$) in heme levels relative to untreated cells (Fig. 3*B*). Cells grown in iron-free media and in the BPS iron chelator control also exhibited significantly reduced heme levels by 70% ($P = 0.006$) and 75% ($P = 0.001$), respectively, relative to untreated cells. These results show that the *P. insularum* homogenate reduced heme synthesis via an iron-dependent mechanism.

The results thus far suggest iron chelation, so we next directly measured iron chelation using the cell-free chrome azurol S (CAS) assay. In this assay, iron chelation is indicated with a blue-to-yellow color transformation (30). Because the pink color of iron-chelated BPS obscures the blue-to-yellow color change, we used EDTA as the positive control. Indistinguishable from the EDTA control, the *P. insularum* homogenate chelated iron at 0.5% (v/v) and 1% (v/v) (Fig. 3*C*), which were the same concentrations that significantly inhibited yeast growth (Fig. 1 *C* and *D*), thereby demonstrating that the *P. insularum* homogenate mediates bioactivity via an iron chelation mechanism.

Bioassay-Guided Fractionation Identifies Two Flavonol Glycosides from the P. insularum Homogenate. A major challenge in the field of traditional medicine is to identify the bioactive component from crude extracts (31–33). To identify the bioactive component in the *P. insularum* homogenate used in Samoan traditional medicine, we conducted bioassay-guided fractionation of the homogenate by monitoring subfractions for the rescue of yeast cell growth with iron supplementation in tandem with nuclear magnetic resonance (NMR) spectroscopic analysis of the purified fractions. Initial fractionation of the homogenate used reversed-phase chromatography on a polymeric (polystyrene-divinyl benzene copolymer; HP-20) resin, followed by HP-20ss purification. Further purification was achieved using size-exclusion chromatography (LH20) and then a final purification using reversed-phase octadecyl-derivatized silica (C_{18}) high performance liquid chromatography (HPLC) to yield low milligram quantities (0.4 to 3.3 mg) of the flavonol glycosides rutin and nicotiflorin, the structures of which were determined by NMR analysis (Fig. 4 *A*–*D* and *SI Appendix*, Fig. S4). In
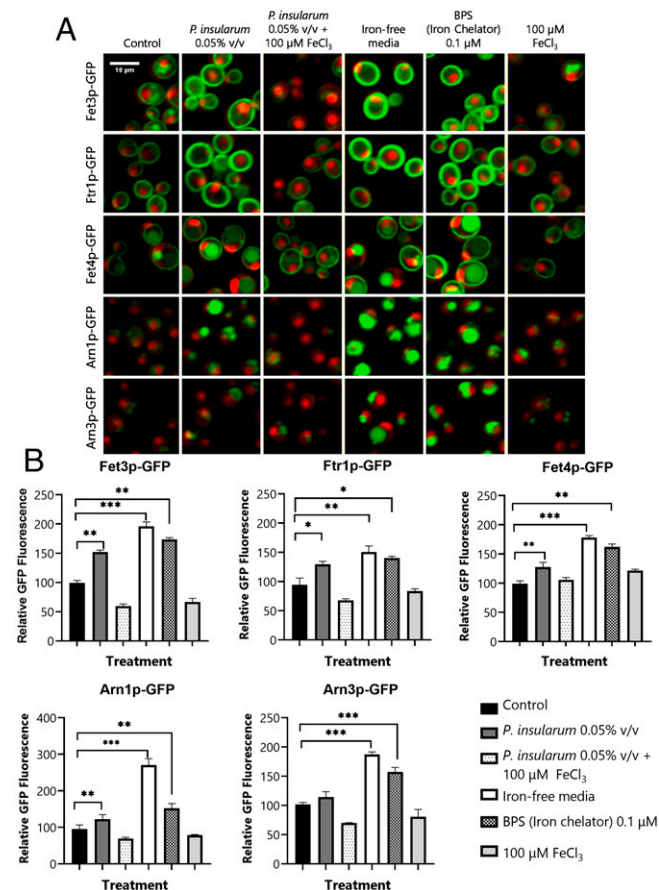

Fig. 2. Protein expression levels of iron transporters are highly responsive to the *P. insularum* homogenate. (*A*) Protein abundance of iron transporters under control (ddH$_2$O) and treatment conditions (0.05% v/v *P. insularum*, 0.05% v/v *P. insularum* homogenate with 100 μM FeCl$_3$ supplementation, iron-free media, 0.1 μM BPS iron chelator, or media supplemented with 100 μM FeCl$_3$) was monitored using confocal fluorescent microscopy analysis of GFP-tagged iron transporters relative to nuclear and cytoplasm markers tagged with high RedStar2 intensity and low-intensity mCherry RFP, respectively. (*B*) Quantification of GFP fluorescence for each of the five iron transporters across the control and the five treatments. GFP quantification of 300 to 400 cells was achieved using ACAPELLA software version 2.0 (PerkinElmer) that identified cells based on the mCherry and RedStar signals and prescribed the quantification of GFP as previously described (25). Three independent experiments with three technical replicates each were conducted. *$P < 0.05$; **$P < 0.01$; ***$P < 0.001$; Student's *t* test comparison to control media.
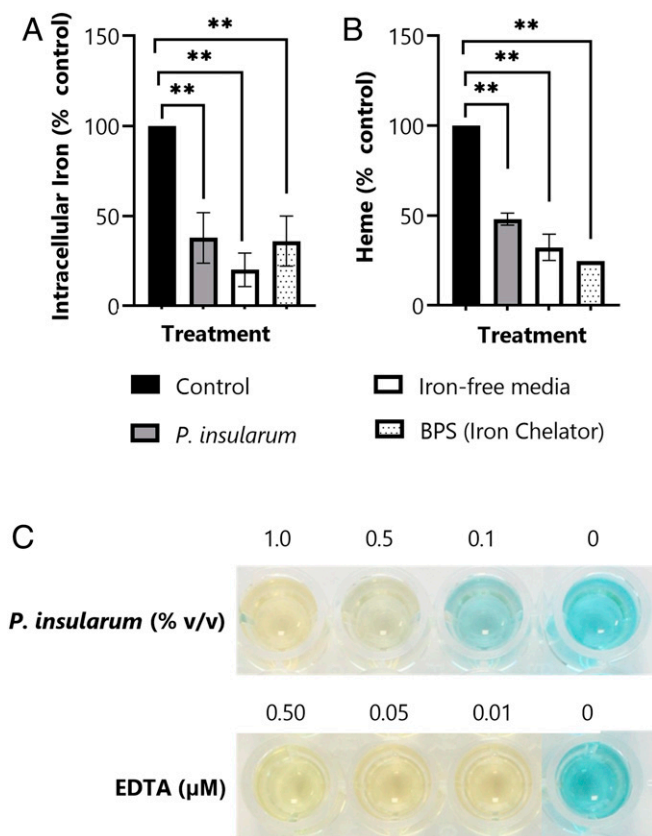
Molimau-Samasoni et al.
Functional genomics and metabolomics advance the ethnobotany of the Samoan traditional medicine "matalafi"

PNAS | 3 of 11
https://doi.org/10.1073/pnas.2100880118

Fig. 3. *P. insularum* treatment impacts iron homeostasis. (*A*) Intracellular iron levels in WT cells grown in control media or treatment media containing 0.05% v/v *P. insularum* homogenate, iron-free media, or 0.1 μM BPS iron chelator. Cells were grown to midlog, lysed, and intracellular iron was quantified using ICP-MS. Results shown are average and SD from three independent experiments with three technical replicates each. **P < 0.01; Student's *t* test comparison to control media. (*B*) Heme levels in WT cells grown in the same conditions as panel *A*. Protein was extracted and heme levels were measured using the triton methanol method via a standard curve with known concentrations of hemin and normalization to control levels. Results presented are the average and SD calculated from three independent experiments with three technical replicates each. **P < 0.01; Student's *t* test comparison to control media. (*C*) Iron chelation activity of the *P. insularum* homogenate compared to EDTA iron chelation was measured in a cell-free CAS assay. A color change from blue to yellow is indicative of iron chelation.

addition, a third bioactive fraction was isolated, although our attempts to characterize this fraction were unsuccessful because of significantly broad, unresolved, aromatic, and aliphatic NMR signals that are characteristic of polymeric flavonoids such as condensed polymeric tannins. To verify our results, NMR spectra of commercial samples of rutin and nicotiflorin were identical with those isolated from *P. insularum* (*SI Appendix*, Fig. S5). Also consistent with the compounds isolated from *P. insularum*, each commercially obtained compound-chelated iron in the CAS assay (*SI Appendix*, Fig. S6). Interestingly, commercially obtained rutin reduced yeast growth at concentrations as low as 63 μM, and this growth defect as well that at higher concentrations was suppressed with iron supplementation, while commercially obtained nicotiflorin did not inhibit yeast growth at the highest 1.7-mM concentration tested (*SI Appendix*, Fig. S7). The lack of growth inhibition bioactivity for authentic nicotiflorin could be explained by the absence of a catechol (*ortho*-dihydroxybenzene), known to reduce metal-chelating ability. Indeed, the iron-chelating activity of nicotiflorin was less than

that of rutin (*SI Appendix*, Fig. S6), suggesting a higher concentration of nicotiflorin is required to elicit growth inhibition in yeast. Nonetheless, nicotiflorin purified from the *P. insularum* homogenate inhibited yeast growth more than the authentic commercial compound, perhaps explained by the presence of minor unresolved compounds seen in the spectra of the purified samples (*SI Appendix*, Fig. S5). In *P. insularum*–derived rutin and nicotiflorin, broad and unresolved resonances around 6.5 ppm within the ^{1}H NMR spectrum are consistent with the presence of condensed tannins, which could explain the distinct bioactivity of *P. insularum*–derived nicotiflorin. Based upon ^{1}H NMR integration values, we estimate the impurity to be between 5 and 10% of each sample, but given the broadness of the signal, it is difficult to determine with certainty.

The *P. insularum* Homogenate Reduces Production of Inflammation-Associated Cytokines by Activated Immune Cells. Iron chelation is involved in many bioactivities including antioxidant, antibacterial, and anti-inflammatory activities (32, 34). To determine if the *P. insularum* homogenate reduces inflammation, for which it is prescribed in traditional Samoan medicine, we compared the effects of varying concentrations of the *P. insularum* homogenate with the bioactive component rutin, the iron chelator BPS, and the anti-inflammatory drug ibuprofen on established mediators of innate and adaptive immunity. Specifically, we selected cytokines that highlighted proinflammatory and anti-inflammatory T helper (Th) subsets: Th1 (cell-mediated immunity), Th2 (wound healing), Th17 (inflammation and antifungal immunity), and regulatory T cells.

To investigate adaptive immunity, cytokines were measured in unstimulated and stimulated splenocytes in the presence of *P. insularum* homogenate, rutin, BPS, or ibuprofen (Fig. 5). The treatments did not reduce viability at any of the tested concentrations (*SI Appendix*, Fig. S8). In unstimulated splenocytes, the baseline production of the Th1-inducing IL12p40 and the fever-inducing cytokine TNFα were significantly reduced with the *P. insularum* homogenate, which was consistent with the activity of rutin, BPS, and ibuprofen. The cytokine IL4, which is critical for Th2-driven wound healing and tissue repair, was significantly increased with ibuprofen, BPS, and rutin treatments, while the *P. insularum* homogenate significantly reduced IL4 levels. In splenocytes stimulated with concanavalin A (ConA) to activate T cells, the *P. insularum* homogenate significantly reduced levels of the Th1 (IFNγ) and Th17 (IL6 and IL17A) proinflammatory cytokines, which aligns with the reduction in baseline IL12p40 and TNFα A similar effect was observed with rutin and ibuprofen, whereas only the Th1 cytokines were affected by BPS. Likewise, splenocytes stimulated with lipopolysaccharide (LPS) to activate B cells exhibited reduced levels of proinflammatory, fever-inducing cytokines (IL1α, IL1β, and IL6) in the Th17 subgroup with *P. insularum* homogenate as well as rutin and to a lesser extent ibuprofen.

To investigate innate immunity, we measured the two main cytokines produced by bone marrow–derived macrophages. The *P. insularum* homogenate significantly increased production of the anti-inflammatory cytokine IL10, significantly reduced production of the proinflammatory Th1-inducing cytokine IL12p40, and also significantly increased viability and proliferation based on the 3-(4,5-dimethylthiazol-2-yl)-2,5-diphenyltetrazolium bromide (MTT) assay (*SI Appendix*, Fig. S9). Notably, BPS and ibuprofen produced a similar IL10 response, albeit to a lesser extent than that observed from the *P. insularum* homogenate. In addition, while BPS treatment significantly downregulated IL12p40 production, ibuprofen failed to show the same effect. Together, these results indicate the *P. insularum* homogenate and the bioactive component rutin reduce proinflammatory and fever-inducing pathways while increasing anti-inflammatory pathways, which are both consistent with
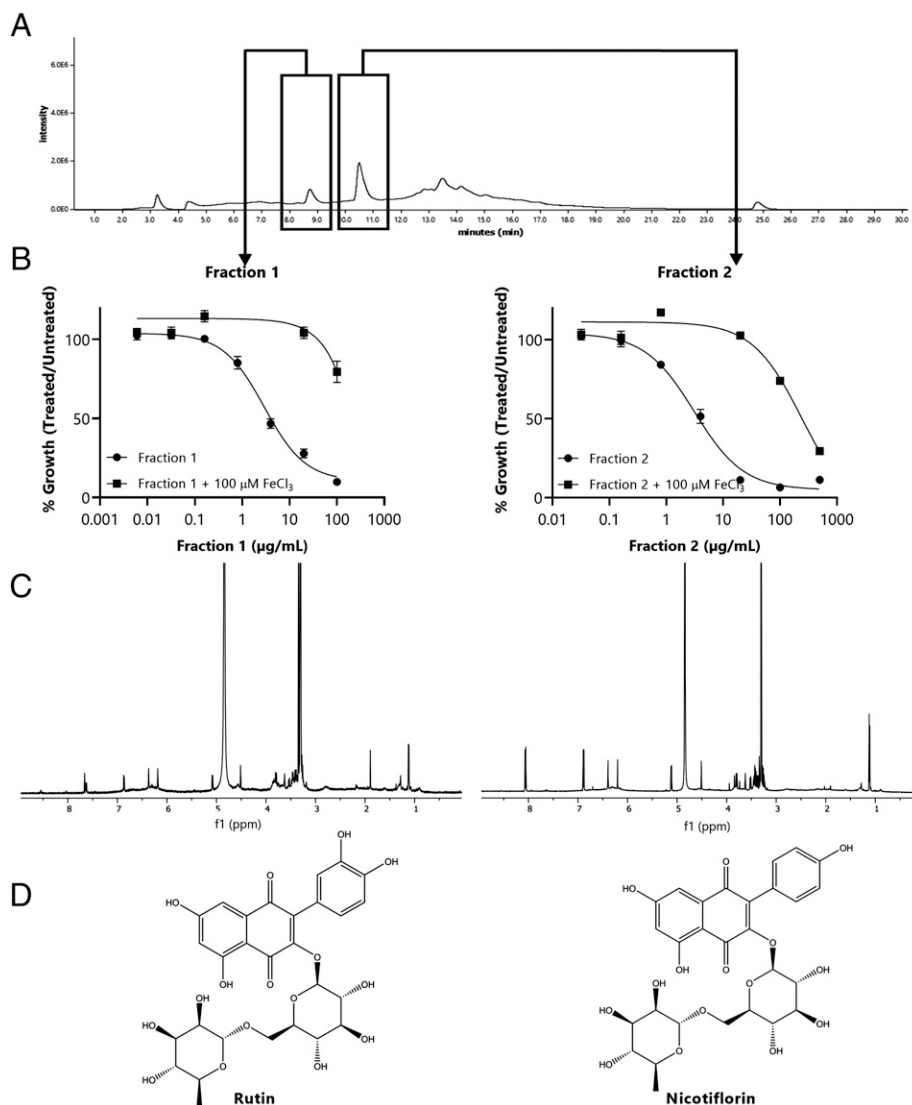
Fig. 4. Bioactivity-guided HPLC purification and NMR analyses led to the isolation and identification of rutin and nicotiflorin. The purification of *P. insularum* homogenate was tracked using a bioassay-guided approach in tandem with NMR analyses. (*A*) The HPLC chromatogram, monitored at 254 nm, showing the two peaks (boxed) that exhibited bioactivity. (*B*) Percent growth of WT yeast in increasing concentrations of HPLC fraction 1 or 2 with the absence or addition of 100 μM FeCl₃ compared to growth in media without each fraction. (*C*) The ¹H NMR (600 MHz, CD₃OD) spectrum of each fraction was subsequently identified as (*D*) rutin and nicotiflorin.

traditional use of the *P. insularum* homogenate to reduce inflammation, reduce fever, and enhance wound-healing.

LC-MS/MS Metabolomics Confirm Iron Chelation Activity of Rutin and Nicotiflorin. To confirm the ability of rutin and nicotiflorin to chelate iron, we used liquid chromatography with tandem mass spectrometry (LC-MS/MS) metabolomics analysis with postcolumn pH adjustment and addition of iron to the column eluent along with ion identity molecular networking within the Global Natural Product Social Molecular Networking (GNPS) platform to detect iron-chelating compounds (35, 36). This analysis identifies defined mass offsets of metal-bound molecular ions relative to their metal-free counterparts. Both pure compounds (rutin, m/z 611.162; nicotiflorin, m/z 595.166) were detected as Fe-bound dimers $[2M + Fe + 2H]^+$ (rutin dimer + Fe, m/z 1,274.226; nicotiflorin dimer + Fe, m/z 1,242.239) when run with iron addition (Fig. 6*A*). These peaks were absent in control experiments without cation supplementation. The detected peak area of the rutin–iron adduct ion was roughly one order of

magnitude greater than that of the nicotiflorin–iron adduct (Fig. 6*B*), with both analyzed at the same concentration. Given their structural similarity and therefore a likely similar ionization response factor, this implies faster binding kinetics for rutin over nicotiflorin. Overall, these findings confirm that rutin and nicotiflorin contribute to the iron chelation mechanism of the *P. insularum* homogenate.

Discussion

Natural products for human diseases have always been important, and traditional remedies such as Samoan medicinal plants have significantly added to this armamentarium (5–13). Here, we have added to this knowledge base by ascertaining the mechanism of action of a traditional Samoan medicinal plant (*P. insularum*); we identified and correlated mechanism of action with the traditional use of the medicine and ultimately determined bioactive principles. First, we used haploinsufficiency genomic analysis in yeast to determine that iron availability was
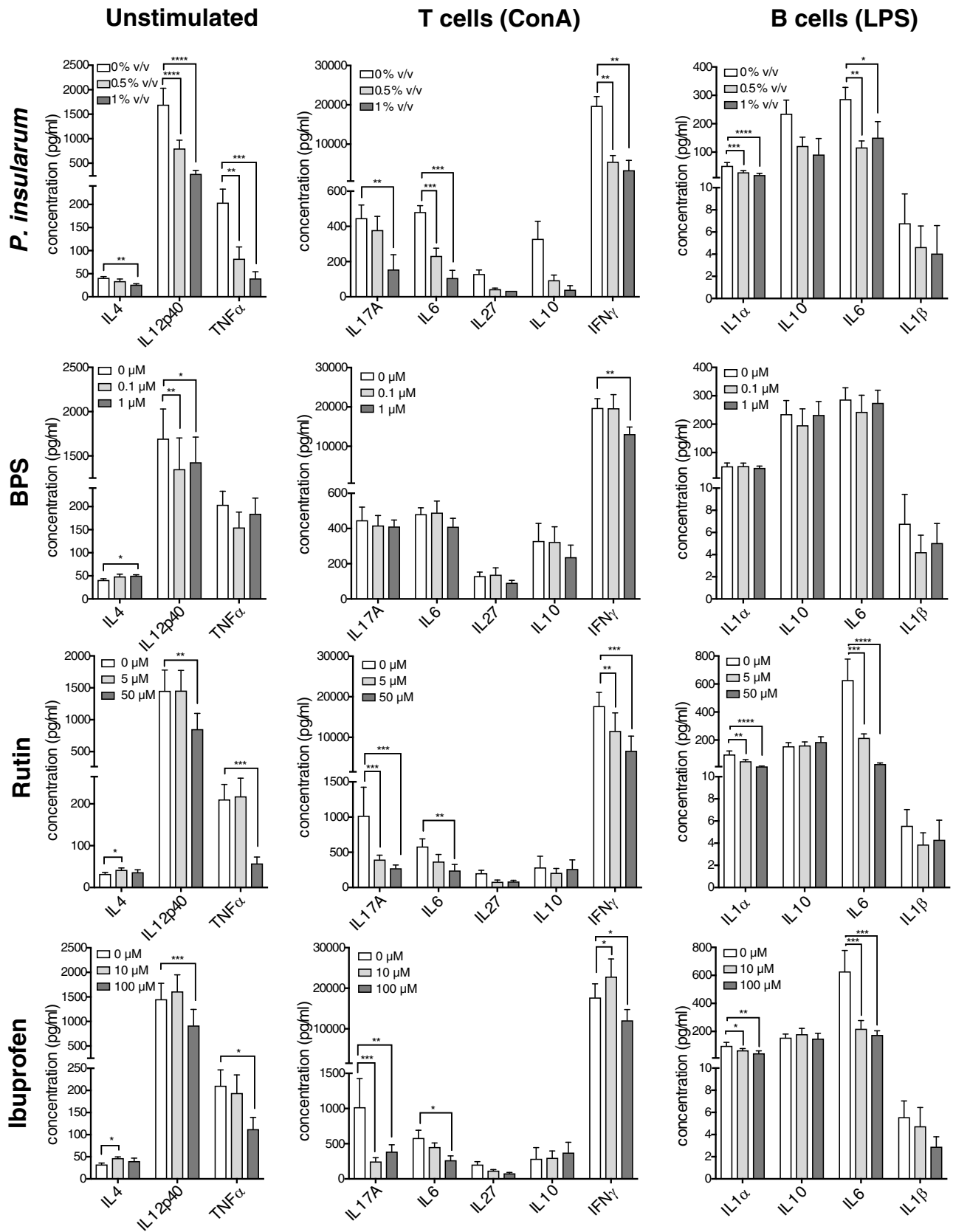
Molimau-Samasoni et al.
Functional genomics and metabolomics advance the ethnobotany of the Samoan traditional medicine "matalafi"

PNAS | 5 of 11
https://doi.org/10.1073/pnas.2100880118

Fig. 5. Anti-inflammatory activity of *P. insularum* homogenate on activated murine immune cells. Cytokine production by unstimulated splenocytes (baseline responses), ConA-stimulated splenocytes (T cell activation; 72 h) and LPS-stimulated splenocytes (B cell activation; 72 h) in the presence of *P. insularum* homogenate, the bioactive component rutin, the iron chelator BPS, and the anti-inflammatory drug ibuprofen. Shown are the mean and SE from three independent biological replicates; each independent replicate performed with splenocytes pooled from three animals. *$P < 0.05$; **$P < 0.01$; ***$P < 0.001$; ****$P < 0.0001$; repeated-measure two-way ANOVA followed by Sidak's multiple comparison test compared to vehicle treatment.

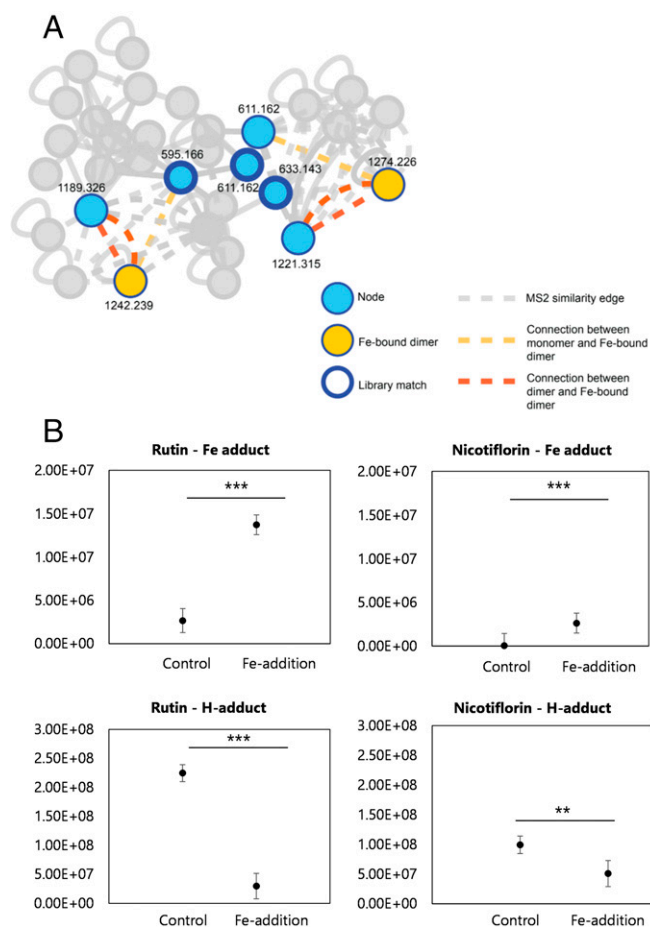Molimau-Samasoni et al.
Functional genomics and metabolomics advance the ethnobotany of the Samoan
traditional medicine "matalafi"

Fig. 6. Native spray metal metabolomics network identifies iron-binding activity of rutin and nicotiflorin. (*A*) Post-LC infusion of Fe^{3+} or H^+ with subsequent MS/MS-based GNPS analysis highlights rutin and nicotiflorin were the only compounds in the full network to complex with iron based on ion identity molecular networking. Edges are based on MS/MS similarity (gray in the absence of binding iron). Both pure compounds (rutin, *m/z* 611.162; nicotiflorin, *m/z* 595.166) were detected to bind iron as dimers with strong connections to monomeric (yellow edges) and dimeric (orange edges) molecular ions of each compound alone, with these peaks absent in control experiments without iron supplementation. Nodes corresponding to binding of an H^+ ion (blue) are shown with a thick outline representing a library match to MoNA MS/MS library in GNPS. (*B*) Integrated peak intensities of dimer peak (2M + H adduct) and iron-bound dimer peak (2M + Fe − 2H adduct) in the control (no infusion) and Fe-infusion samples. Shown are the results from three replicates with the average indicated with a horizontal line. Statistical significance between integrated peak areas was calculated using a Student's *t* test (*$P < 0.05$; **$P < 0.01$).

integral to the mechanism of action of the *P. insularum* homogenate. We described a bioassay-guided fractionation scheme that led to the discovery of bioactive iron chelators, rutin and nicotiflorin, in the *P. insularum* homogenate. The anti-inflammatory effects of the *P. insularum* homogenate and rutin on unstimulated splenocytes, ConA-activated T cells, and LPS-activated B cells were as potent as the anti-inflammatory drug ibuprofen. The similarity in the anti-inflammatory activity of the *P. insularum* homogenate with the extensively used ibuprofen would be consistent with the diverse uses of the *P. insularum* homogenate in Samoan traditional medicine. Overall, using a crude traditional homogenate with methodology integrating genomics, metabolomics, analytical chemistry and immunology, we identified 1) a mechanism of action that underpinned the traditional

anti-inflammatory remedy and 2) potential applications of the traditional medicine not previously informed by traditional knowledge.

Our results fit and extend an established system using yeast as a model system for elucidating mechanisms of iron metabolism in humans (20–23). For example, the natural product and first-line treatment for type 2 diabetes prescribed for 150 million persons worldwide, metformin, was shown in yeast to induce an iron-deficiency state (37, 38). Indeed, iron chelators, such as deferasirox, deferiprone, and deferoxamine, initially approved for iron overload disorders associated with transfusions impacting 1.62 billion people (39), are also now described as prospective agents against common diseases such as cancer (40), neurodegenerative diseases (41), cardiovascular disease (42), and diabetes (43). As inflammation and iron chelation are fundamental to these diseases (44–46), this raises the possibility for applications of *P. insularum* beyond traditional use.

We identified rutin and nicotiflorin as bioactive components of *P. insularum* homogenate in treating inflammation and associated symptoms in Samoan traditional medicine. More broadly, our findings fit with anti-inflammatory and neuroprotective effects of rutin and nicotiflorin in treating neurodegenerative diseases such as Parkinson's and Alzheimer's (47–49). These results reiterate that rutin and nicotiflorin are bioactive compounds of current interest and moreover suggest that there may be uses for the *P. insularum* homogenate not informed by traditional use in Samoa but informed here with unbiased chemical genomic analyses. While there is no record of *P. insularum* in a traditional use against hyperlipidemia-associated diseases, our chemical genomic analysis highlighted the sensitivity of the RIM101 gene deletion to the *P. insularum* homogenate. RIM101 in yeast is a major regulator of lipotoxicity, the process of lipid-dependent cell death that is associated with obesity, diabetes, and cardiovascular disease (50). This observation may be of direct relevance to Samoa given the genetic predisposition to obesity in Samoa (51). Also of current interest, molecular docking studies of 33 molecules predicted rutin as the strongest contender in binding the active site of the SARS-CoV-2 main 3C-L protease for inhibiting viral replication and potentially treating the COVID-19 pandemic (52). Antilipotoxicity and antiviral activities by rutin are not unprecedented (53–56), albeit not used to date to inform new uses of traditional medicine. Our results thus broaden the therapeutic potential and applications of *P. insularum* in Samoan traditional medicine.

It is also plausible that the iron chelation activity of the *P. insularum* homogenate (by rutin, nicotiflorin, and other condensed tannins) inhibits ferroptosis, an iron-dependent programmed cell death triggered by intracellular phospholipid peroxidation. Pathological cell death associated with several diseases including inflammation, Alzheimer's, Parkinson's, and Huntington's diseases, periventricular leukomalacia, renal insufficiency, carcinogenesis, and kidney degeneration have shown hallmarks of ferroptosis (57). Regulating ferroptosis through iron chelation becomes a potential management tool for these diseases. Ferroptosis is a fairly new categorization and not yet well-studied when it comes to traditional medicine, with only a few studies in traditional Chinese medicine (58). Given flavonoids are prominent components of many plant extracts used in traditional medicine, it would be interesting to determine if antioxidant and iron chelation mechanisms mediating antiferroptosis activity are also mechanisms amenable to traditional medicine.

To further develop the *P. insularum* homogenate, additional analyses of natural variation in the chemical biology of *P. insularum* must be investigated. Spatial and temporal variation can lead to differences in chemical composition, but also cultivar differences have been shown to alter the levels and types of flavonoids present within plants (59). As the *P. insularum* in our

Molimau-Samasoni et al.
Functional genomics and metabolomics advance the ethnobotany of the Samoan traditional medicine "matalafi"

PNAS | 7 of 11
https://doi.org/10.1073/pnas.2100880118

study was collected from *P. insularum* cultivated by a traditional healer, future studies should include *P. insularum* collected from cultivated as well as wild sources in Samoa and additionally wild *P. insularum* from other South Pacific islands, where interestingly, *P. insularum* is not reportedly used in traditional medicine. Likewise, a pharmacodynamic understanding of *P. insularum* is necessary. Since iron chelators alter the microbiome and immune cells respond to microbiota (60), it is plausible that the *P. insularum* homogenate consumed orally alters the intestinal microbiome, which could also mediate additional effects of the homogenate.

This study incorporated sophisticated yeast chemical genomic analyses to identify the biological mechanism of action of a traditional medicine as a whole entity as prepared by traditional healers, and this mechanism was then monitored in bioactivity-guided fractionation to identify the bioactive components. This combinatorial approach provides molecular insight into traditional knowledge and provides insight into potential new uses of traditional medicine. As recently deemed to be increasingly important for advancing ethnobiology and natural product drug discovery, albeit rarely accomplished (61–63), our study integrated indigenous researcher–community engagement with interdisciplinary methodologies to discover and develop the great pharmaceutical potential in traditional knowledge regarding natural products as used in traditional medicine.

Materials and Methods

Plant Collection. Leaves were collected in 2013 and 2018 from an individual *P. insularum* plant (GPS coordinates: Latitude S 13°48′53″, Longitude W 171°53′6″) via engagement with Seti Fa'aifo, the landowner of the property and distant relative to S.M.S. Both Seti Fa'aifo and botanist S.T.F. positively identified *P. insularum*. Permit for plant collection was provided by the Ministry of Natural Resources and Environment (MNRE) in Samoa. Voucher specimen (SROS_2021_407) has been deposited at Scientific Research Organisation of Samoa (SROS).

Leaf Homogenate Preparation. Within an hour after collection, leaves were washed with sterile water, processed through a juicer (Breville BJE200), and the resulting leaf juice was transported on ice to Wellington, New Zealand, for analysis under the auspices of the MNRE permit, the memorandum of understanding between SROS and Victoria University of Wellington, and the import permit from the Ministry of Primary Industries New Zealand. The juice was centrifuged, and the supernatant was treated as the homogenate after a final filtration through a 0.2-μm filter with a 30-mm polyethersulfone membrane (Biofil).

Strains, Media, and Chemicals. All yeast strains used in this study were in the BY4741 background. Haploid yeast deletion strains (MATa; Open Biosystems) carrying the geneticin-selectable marker were maintained on yeast peptone dextrose (YPD) medium containing 200 μg/mL geneticin (Life Technologies). GFP/RFP-tagged yeast strains were maintained on synthetic complete media buffered to pH 7 with 25 mM HEPES (SCH) without histidine (selection for GFP) and containing hygromycin and nourseothricin antibiotics (selection for RFP) (26). HEPES was purchased from Formedium. BPS, rutin, cycloheximide, atorvastatin and ibuprofen were purchased from Sigma-Aldrich. Nicotiflorin was supplied by AvaChem Scientific. EDTA was purchased from AppliChem GmbH.

Chemical Genomic Analysis. An aliquot of a pooled heterozygous deletion library of yeast (Open Biosystems) was treated with 0.005% v/v of the *P. insularum* homogenate for 20 generations at 30 °C. Genomic DNA from treated cells was isolated using YeaStar Genomic DNA Kit (ZymoResearch). Then the unique 20-bp barcodes flanking each gene deletion (UPTAG upstream and DNTAG downstream of each gene deletion) were amplified, sequenced, demultiplexed, and quantified to record logFC, FDR, and logCPM for every gene deletion of the heterozygous library as previously described (64).

Functional Enrichment Analysis. Over-representation of genes sensitive to the *P. insularum* homogenate for specific GO terms in the molecular function category was investigated using YeastEnrichr (19). Significant enrichment was defined via an enrichment score that integrates the log of the *P* less than 0.05

from the Fisher exact test for random gene sets and the *z*-score of the deviation of the observed rank for each GO term in the *P. insularum* homogenate-sensitive gene set from the expected rank for each term.

Metal Rescue Assay. Yeast cultures at 5×10^5 cells/mL were grown in SCH and supplemented with or without $FeCl_3$, $FeSO_4$, or $ZnCl_2$ together with increasing concentrations of *P. insularum* homogenate. Cells were subsequently incubated at 30 °C until control cells reached midlog (optical density [OD] = 0.4 to 0.6) and then quantified via absorbance at 590 nm using a PerkinElmer Envision plate reader.

Intracellular Iron Quantification. Yeast cultures at 5×10^5 cells/mL were grown in SCH at 30 °C until control cells reached midlog (OD = 0.4 to 0.6), and intracellular iron was measured in yeast cells using ICP-MS as previously described (27). Briefly, cells were digested in 3% nitric acid at 96 °C for 16 h, supernatant was collected, and iron content was quantified using Element 2 High Resolution ICP-MS (Thermo Scientific).

Confocal Fluorescence Microscopy. Protein expression was quantified by fluorescence of a GFP-tagged protein of interest relative to the RFP fluorescence of internal markers of the cytoplasm and nucleus (mCherry and RedStar, respectively). Strains were grown in liquid SCH with and without *P. insularum* homogenate at 30 °C for 15 h, diluted to ~1×10^8 cells/mL, transferred to 384 clear bottom microtitre plates (PerkinElmer), and visualized using a high-throughput spinning disk confocal microscope (General Electric IN Cell Analyzer 6500HS with 60× (numerical aperture 0.9) air objective for screening 84 GFP-tagged strains or PerkinElmer Opera with 60× (numerical aperture 1.2) water objective for select GFP-tagged strains). GFP excitation was at 488 nm and detected with a 520/35 filter. mCherry and RedStar excitation was at 561 nm and detected with a 600/40 filter. An exposure of 400 ms with five Z-stacks 0.5 μm apart was used for all images. GFP quantification of 300 to 400 cells was achieved using ACAPELLA software version 2.0 (PerkinElmer) that identified cells based on the mCherry and RedStar signals and prescribed the quantification of GFP as previously described (26).

Heme Quantification. Yeast cultures at 5×10^5 cells/mL were grown in SCH at 30 °C until control cells reached midlog (OD = 0.4 to 0.6), and protein was extracted as previously described (65). Heme was then quantified by the triton-methanol protocol as previously described (29). In brief, equal amounts of clarified cell lysate was added to 5% triton in methanol, absorbance was read at 405 nm using a PerkinElmer Envision plate reader, and heme was quantified relative to a hemin (Sigma-Aldrich) standard curve (10 to 500 nM).

Colorimetric Iron Chelation Assay. Iron chelation was directly measured using a modified CAS assay as previously described (30). Briefly, a solution comprising CAS, $FeCl_3$, and hexadecyltrimethylammonium bromide was prepared in the presence and absence of various dilutions of *P. insularum* homogenate or EDTA. A color change from blue to yellow was indicative of iron chelation activity.

Mouse Husbandry. Male and female C57BL/6 mice (6- to 12-wk old) were obtained from the Malaghan Institute of Medical Research and housed in the School of Biological Sciences Animal Facility at Victoria University. All experiments with animals were carried out in this animal facility and were approved by the Victoria University of Wellington Animal Ethics Committee (protocols 2014-R23 and 25295).

Immune Response Assays. To assess T cell responses, splenocytes were isolated from C57BL/6 mice as previously described (66) and cultured (1×10^6 cells/well) for 72 h in the presence or absence of ConA (a polyclonal T cell mitogen; 1 μg/mL; Sigma). For each experiment, splenocytes were pooled from three animals, and three independent experiments were performed for each assay. To assess B cell responses, splenocytes were isolated and stimulated for 72 h with LPS (a polyclonal B cell mitogen; 200 ng/mL). Cytokines were measured in the culture supernatants by enzyme-linked immunosorbent assay (BD Biosciences) for IL12p40, IL4, and IL10 according to manufacturer instructions, and plates were read at 450 nm using a multiwell Enspire Multilabel plate reader (PerkinElmer). Additionally, TNFα, IL6, IL27, IL17A, IFNγ, IL1α, and IL1β were measured in culture supernatants from unstimulated, ConA-stimulated, or LPS-stimulated splenocytes using a LEGENDplex Mouse Inflammation Panel 13-plex (Biolegend) by flow cytometry according to manufacturer instructions and acquired on a FACS Canto II flow cytometer (BD Biosciences). Data analysis was conducted using LEGENDplex software (Biolegend). Primary bone marrow–derived macrophage cultures were prepared from C57BL/6 mice as described (67) using IL-3 and GM-CSF (both at 5 ng/mL; Peprotech) for 7 to 10 d. Macrophages (1×10^5 cells/well) were

primed overnight with IFNγ (20 U/mL; Peprotech) before stimulation with LPS (200 ng/mL; Sigma) for 24 h. Cell viability was assessed via MTT assay; briefly, cells were incubated for 2 h with the MTT solution (5 mg/mL; Sigma) before adding the solubilizer (10% sodium dodecyl sulfate, 45% dimethylformamide) overnight, and MTT reduction was measured by absorbance at 550 nm in a multiwell Enspire Multilabel plate reader (PerkinElmer). Statistical significance between multiple groups assessed using repeated-measure two-way ANOVA followed by Sidak's multiple comparison test.

NMR, MS, HPLC, and TLC Analyses for Compound Isolation. NMR analyses were carried out using a Varian Direct Drive 600-MHz NMR spectrometer operating at 600 MHz for ^1H and 150 MHz for ^{13}C nuclei, respectively. Samples were dissolved in deuterated solvent (Cambridge Isotope Labs), and the residual protonated solvent peak was used as an internal reference (CD₃OD: δ_H 3.31, δ_C 49.0; CDCl₃: δ_H 7.21, δ_C 77.0). High-resolution electrospray ionization mass spectrometry (HRESIMS) data were acquired using an Agilent 6530 Accurate-Mass Q-TOF LC-MS equipped with a 1260 Infinity binary pump. Data-dependent electrospray LC-MS/MS analysis was performed with a Q-Exactive orbitrap mass spectrometer (Thermo Scientific) operating in both positive and negative ion modes. HPLC purification was carried out using an Agilent Technologies 1260 Infinity instrument equipped with a quaternary pump and dual detection capability using the diode array and evaporative light scattering detector modules. Thin-layer chromatography (TLC) analyses were performed on Macherey-Nagel Polygram Sil G/UV254 plates and developed by first visualizing under ultraviolet light ($\lambda = 254$ nm), then dipping in 5% H₂SO4/CH₃OH, followed by 0.1% vanillin/ CH₃CH₂OH before heating.

Bioactivity-Guided Fractionation. Filtered *P. insularum* juice (200 mL) was passed through Diaion HP-20 poly(styrene-divinyl benzene) copolymer resin (Supelco) (100 mL) that was pre-equilibrated with three column volumes each of acetone, methanol, and dH₂O. The column was then eluted with three column volumes each of dH₂O, 30, 75, and 100% acetone in dH₂O (v/v), to which bioactivity was predominantly confined to the 75% acetone in dH₂O fraction. The 75% aqueous acetone fraction was then loaded onto Diaion HP-20ss (Supelco) by evaporating the fraction onto HP-20ss (5 mL) and transferring as a slurry in dH₂O onto a larger bed of the stationary phase (15 mL). The column was washed with dH₂O and eluted with three bed volumes each of 30, 40, 50, 60, 75, and 100% acetone in dH₂O. Fractions (10 mL) were collected in test tubes and evaporated *in vacuo*. Bioactive fractions found within the 50% aqueous acetone fraction were further subjected to size-exclusion chromatography using Sephadex LH20 (GE Healthcare Life Sciences) (2.5 × 90 cm) eluting with 50% methanol in dH₂O (v/v, 750 mL) at 17 mL/h collected in bulk, followed by 70% acetone in dH₂O (v/v, 400 mL) at a flow rate of 25 mL/h collecting 5-mL fractions. Fractions were dried *in vacuo*, combined on the basis of TLC analysis (butanol:acetic acid:dH₂O, 4:1:2, v/v), and their iron chelation bioactivity determined. Subsequent purification utilizing reversed-phase HPLC with octadecyl-derivatized silica (C₁₈) (Phenomenex Prodigy: 4.6 × 250 mm, 5 μm) and a binary gradient solvent system consisting of increasing volumes of acetonitrile in dH₂O (0 to 10 min, 20 to 30% acetonitrile in dH₂O; 10 to 20 min, held at 30% acetonitrile in dH₂O; 20 to 23 min, 30 to 90% acetonitrile in dH₂O; 23 to 30 min, held at 90% acetonitrile in dH₂O) resulted in the isolation of rutin (0.4 mg; Rt 8.9 min) and nicotiflorin (3.3 mg; Rt 10.2 min). HRESIMS provided the deprotonated molecular ion for rutin *m/z* 609.1458 [M-H]⁻ (calcd C₂₇H₂₉O₁₆ *m/z* 609.1459, $\Delta = -0.3$ ppm) and nicotiflorin *m/z* 593.1509 [M-H]⁻ (calcd C₂₇H₂₉O₁₅ *m/z* 593.1512, $\Delta = -0.44$ ppm), respectively. Full NMR characterization of purified compounds was performed and validated by comparison of NMR data with that of authentic commercial standards.

LC-MS/MS Iron-Binding Metabolomics (Data Acquisition). Binding of iron by small molecules was detected using Ion Identity Molecular Networking metabolomics as previously described (36). For microflow UHPLC-MS/MS analysis, samples were dissolved in 80% methanol (to a final concentration of 100 μg/ mL) and 5 μL was injected into a Vanquish UHPLC system coupled to a Q-Exactive quadrupole orbitrap mass spectrometer (Thermo Fisher Scientific) with an Agilent 1260 quaternary HPLC pump (Agilent) as a makeup pump. For reversed-phase chromatography, a C₁₈ core-shell microflow column (Kinetex C₁₈, 50 × 1 mm, 1.8-μm particle size, 100-A pore size, Phenomenex) was used. The mobile phase consisted of solvent A (H₂O + 0.1% formic acid) and solvent B (acetonitrile + 0.1% formic acid). The flow rate was set to 100 μL/min. A linear gradient from 5 to 50% B between 0 to 4 min and 50 to 99% B between 4 to 6 min, followed by a 2-min washout phase at 99% B and a 4-min re-equilibration phase at 5% B. Data-dependent acquisition of MS/MS spectra was performed in positive mode. Makeup flow of ammonium acetate buffer (10 mM) + 0.2% ammonium hydroxide was set to 100 μL/min and infused

postcolumn through a peak T-splitter. Iron chloride (FeCl₃) was infused postcolumn and postmakeup through a second T-splitter at a flow rate of 5 μL/min and a concentration of 1 mM. Electrospray ionization (ESI) parameters were set to 40 arbitrary units (AU) sheath gas flow, auxiliary gas flow was set to 10 AU, and sweep gas flow was set to 0 AU. Auxiliary gas temperature was set to 400 °C. The spray voltage was set to 3.5 kV and the inlet capillary was heated to 320 °C. S-lens level was set to 70 V applied. MS scan range was set to 200 to 2,000 *m/z* with a resolution at *m/z* 200 (R*m/z* 200) of 70,000 with one microscan. The maximum ion injection time was set to 100 ms with automatic gain control (AGC) target of 5.0E5. Up to two MS/MS spectra per duty cycle were acquired at R*m/z* 200 17,000 with one microscan. The maximum ion injection time for MS/MS scans was set to 100 ms with an AGC target of 5.0E5 ions and a minimum 5% AGC. The MS/MS precursor isolation window was set to *m/z* 1. The normalized collision energy was stepped from 20 to 30 to 40% with z = 1 as default charge state. MS/MS scans were triggered at the apex of chromatographic peaks within 2 to 15 s from their first occurrence. Dynamic precursor exclusion was set to 5 s. Ions with unassigned charge states were excluded from MS/MS acquisition as well as isotope peaks.

LC-MS/MS Iron-Binding Metabolomics (Data Analysis). Feature finding and ion identity networking were performed using an in-house modified version of MZmine2.37 (68), corr.17.7 available at https://github.com/robinschmid/ mzmine2/releases. Feature tables, MS/MS spectra files (mgf), and ion identity networking results were exported, uploaded to the MassIVE repository, and submitted to GNPS (35) for feature-based molecular networking analysis.

MS/MS spectra were converted to .mzML files using MSconvert (ProteoWizard) (69). All raw and processed data are publicly available at ftp://massive. ucsd.edu/MSV000086287/. MS1 feature extraction and MS/MS pairing were performed with MZmine 2.37 (68) corr17.7_kai_merge2. An intensity threshold of 1E5 for MS1 spectra and of 1E3 for MS/MS spectra was used. MS1 ADAP chromatogram building was performed within a 10 ppm mass window and a minimum peak intensity of 3E5 was set. Extracted Ion Chromatograms (XICs) were deconvoluted using baseline cutoff with *m/z* range for MS2 pairing of 0.01 and RT range for MS2 scan pairing of 0.2. After chromatographic deconvolution, MS1 features linked to MS/MS spectra within 0.01 *m/z* mass and 0. 2 min retention time windows. Isotope peaks were grouped and features from different samples were aligned with 10 ppm mass tolerance and 0.2 min retention time tolerance. MS1 peak lists were joined using an *m/z* tolerance of 10 ppm and retention time tolerance of 0.1 min; alignment was performed by placing a weight of 75 on *m/z* and 25 on retention time. Correlation of coeluting features was performed with the metaCorrelate module; retention time tolerance of 0.1, minimum height of 1E5 and noise level of 1E5 were used. A correlation of 0.85 was set as the threshold for the min feature shape corr., and feature height correlation was not used. The following adducts were searched: [M + H⁺]⁺, [M + Na⁺]⁺, [M + K⁺]⁺, [M + NH]²⁺, [M + Fe³⁺ - 2H⁺]⁺, with an *m/z* tolerance of 10 ppm, a maximum charge of 2, and maximum molecules/cluster of 2.

Peak areas and feature correlation pairs were exported as .csv files and the corresponding consensus MS/MS spectra were exported as an .mgf file. For spectral networking and spectrum library matching, all files were uploaded to the feature-based molecular networking workflow on GNPS (35) (https://gnps. ucsd.edu/ProteoSAFe/static/gnps-splash.jsp). For spectrum library matching and spectral networking, the minimum cosine score to define spectral similarity was set to 0.7. The Precursor and Fragment Ion Mass Tolerances were set to 0.01 Da and Minimum Matched Fragment Ions to 4, Minimum Cluster Size to 1 (MS Cluster off). When analog search was performed, the maximum mass difference was set to 100 Da. The GNPS job can be accessed at https://gnps. ucsd.edu/ProteoSAFe/status.jsp?task=76115ecaad9c46e9aaa30413d0d435eb. Molecular networks were visualized with Cytoscape 3.7.1 (70).

The XCalibur Quant Browser (Thermo) was used to obtain integrated peak areas of both apo- and iron-bound adducts. The XCalibur processing method integrates exact mass +/− 10 ppm, utilizing ICIS Peak Detection with 7 smoothing points, a baseline window of 40, area noise factor of 5, and peak noise factor of 6. Statistical significance between integrated peak areas was calculated using an unpaired *t* test.

Data Availability. Feature finding and ion identity networking were performed using an in-house modified version of MZmine2.37 (68), corr.17.7 available at GitHub, https://github.com/robinschmid/mzmine2/releases. Feature tables, MS/MS spectra files (mgf), and ion identity networking results were exported, uploaded to the MassIVE repository (https://massive.ucsd.edu/ ProteoSAFe/dataset_files.jsp?task=16c65622121c488d9123dc42c556dbff#%7 B%22table_sort_history%22%3A%22main.collection_asc%22%2C%22main. collection_input%22%3A%22metadata%7C%7CEXACT%22%7D), and submitted to GNPS (35) (https://gnps.ucsd.edu/ProteoSAFe/status.jsp?task=76115

Molimau-Samasoni et al.
Functional genomics and metabolomics advance the ethnobotany of the Samoan traditional medicine "matalafi"

PNAS | 9 of 11
https://doi.org/10.1073/pnas.2100880118

1. D. J. Newman, G. M. Cragg, Natural products as sources of new drugs over the nearly four decades from 01/1981 to 09/2019. *J. Nat. Prod.* **83**, 770–803 (2020).
2. A. L. Harvey, Natural products in drug discovery. *Drug Discov. Today* **13**, 894–901 (2008).
3. D. A. Dias, S. Urban, U. Roessner, A historical overview of natural products in drug discovery. *Metabolites* **2**, 303–336 (2012).
4. Y. Tu, The discovery of artemisinin (qinghaosu) and gifts from Chinese medicine. *Nat. Med.* **17**, 1217–1220 (2011).
5. K. R. Gustafson *et al.*, A nonpromoting phorbol from the samoan medicinal plant *Homalanthus nutans* inhibits cell killing by HIV-1. *J. Med. Chem.* **35**, 1978–1986 (1992).
6. E. J. Beans *et al.*, Highly potent, synthetically accessible prostratin analogs induce latent HIV expression *in vitro* and *ex vivo*. *Proc. Natl. Acad. Sci. U.S.A.* **110**, 11698–11703 (2013).
7. M. G. Desimio, E. Giuliani, A. S. Ferraro, G. Adorno, M. Doria, *In vitro* exposure to prostratin but not bryostatin-1 improves natural killer cell functions including killing of CD4+ T cells harbouring reactivated human immunodeficiency virus. *Front. Immunol.* **9**, 1514 (2018).
8. A. W. Whistler, *Samoan Herbal Medicine* (Isle Botanica, Honolulu, HI, 1996).
9. L. Castro, K. Tsuda, *Samoan Medicinal Plants and Their Usage* (Agricultural Development in the American Pacific Project, University of Hawai'i at Manoa, 2001)
10. P. A. Cox *et al.*, Pharmacological activity of the Samoan ethnopharmacopoeia. *Econ. Bot.* **43**, 487–497 (1989).
11. T. R. Norton *et al.*, Pharmacological evaluation of medicinal plants from Western Samoa. *J. Pharm. Sci.* **62**, 1077–1082 (1973).
12. C. A. Dunstan *et al.*, Evaluation of some Samoan and Peruvian medicinal plants by prostaglandin biosynthesis and rat ear oedema assays. *J. Ethnopharmacol.* **57**, 35–56 (1997).
13. A. Frankova *et al.*, *In vitro* antibacterial activity of extracts from Samoan medicinal plants and their effect on proliferation and migration of human fibroblasts. *J. Ethnopharmacol.* **264**, 113220 (2021).
14. S. L. Gerlach, R. Burman, L. Bohlin, D. Mondal, U. Göransson, Isolation, characterization, and bioactivity of cyclotides from the Micronesian plant *Psychotria leptothyrsa*. *J. Nat. Prod.* **73**, 1207–1213 (2010).
15. S. L. Gerlach *et al.*, A systematic approach to document cyclotide distribution in plant species from genomic, transcriptomic, and peptidomic analysis. *Biopolymers* **100**, 433–437 (2013).
16. M. E. Hillenmeyer *et al.*, The chemical genomic portrait of yeast: Uncovering a phenotype for all genes. *Science* **320**, 362–365 (2008).
17. A. Y. Lee *et al.*, Mapping the cellular response to small molecules using chemogenomic fitness signatures. *Science* **344**, 208–211 (2014).
18. F. Zhang *et al.*, A marine microbiome antifungal targets urgent-threat drug-resistant fungi. *Science* **370**, 974–978 (2020).
19. M. V. Kuleshov *et al.*, Enrichr: A comprehensive gene set enrichment analysis web server 2016 update. *Nucleic Acids Res.* **44**, W90–W97 (2016).
20. D. J. Eide, The molecular biology of metal ion transport in *Saccharomyces cerevisiae*. *Annu. Rev. Nutr.* **18**, 441–469 (1998).
21. M. R. Bleackley, R. T. A. Macgillivray, Transition metal homeostasis: From yeast to human disease. *Biometals* **24**, 785–809 (2011).
22. D. M. De Silva, C. C. Askwith, D. Eide, J. Kaplan, The FET3 gene product required for high affinity iron transport in yeast is a cell surface ferroxidase. *J. Biol. Chem.* **270**, 1098–1101 (1995).
23. R. Stearman, D. S. Yuan, Y. Yamaguchi-Iwai, R. D. Klausner, A. Dancis, A permease-oxidase complex involved in high-affinity iron uptake in yeast. *Science* **271**, 1552–1557 (1996).
24. A. M. Smith, C. Ammar, C. Nislow, G. Giaever, A survey of yeast genomic assays for drug and target discovery. *Pharmacol. Ther.* **127**, 156–164 (2010).
25. C. C. Philpott, O. Protchenko, Response to iron deprivation in *Saccharomyces cerevisiae*. *Eukaryot. Cell* **7**, 20–27 (2008).
26. P. W. Bircham *et al.*, Secretory pathway genes assessed by high-throughput microscopy and synthetic genetic array analysis. *Mol. Biosyst.* **7**, 2589–2598 (2011).
27. J. Tamarit, V. Irazusta, A. Moreno-Cermeño, J. Ros, Colorimetric assay for the quantitation of iron in yeast. *Anal. Biochem.* **351**, 149–151 (2006).
28. H. Lange, G. Kispal, R. Lill, Mechanism of iron transport to the site of heme synthesis inside yeast mitochondria. *J. Biol. Chem.* **274**, 18989–18996 (1999).
29. A. V. Pandey, S. K. Joshi, B. L. Tekwani, V. S. Chauhan, A colorimetric assay for heme in biological samples using 96-well plates. *Anal. Biochem.* **268**, 159–161 (1999).
30. D. B. Alexander, D. A. Zuberer, Use of chrome azurol S reagents to evaluate siderophore production by rhizosphere bacteria. *Biol. Fertil. Soils* **12**, 39–45 (1991).

31. A. Harvey, Strategies for discovering drugs from previously unexplored natural products. *Drug Discov. Today* **5**, 294–300 (2000).
32. J. D. Phillipson, Phytochemistry and medicinal plants. *Phytochemistry* **56**, 237–243 (2001).
33. J. L. Wolfender, G. Marti, A. Thomas, S. Bertrand, Current approaches and challenges for the metabolite profiling of complex natural extracts. *J. Chromatogr. A* **1382**, 136–164 (2015).
34. B. J. Crielaard, T. Lammers, S. Rivella, Targeting iron metabolism in drug discovery and delivery. *Nat. Rev. Drug Discov.* **16**, 400–423 (2017).
35. M. Wang *et al.*, Sharing and community curation of mass spectrometry data with Global Natural Products Social Molecular Networking. *Nat. Biotechnol.* **34**, 828–837 (2016).
36. R. Schmid *et al.*, Ion identity molecular networking for mass spectrometry-based metabolomics in the GNPS environment. *Nat. Commun.* **12**, 3832 (2021).
37. L. He, S. Meng, E. L. Germain-Lee, S. Radovick, F. E. Wondisford, Potential biomarker of metformin action. *J. Endocrinol.* **221**, 363–369 (2014).
38. B. Stynen *et al.*, Changes of cell biochemical states are revealed in protein homomeric complex dynamics. *Cell* **175**, 1418–1429.e9 (2018).
39. R. E. Fleming, P. Ponka, Iron overload in human disease. *N. Engl. J. Med.* **366**, 348–359 (2012).
40. S. V. Torti, F. M. Torti, Iron and cancer: More ore to be mined. *Nat. Rev. Cancer* **13**, 342–355 (2013).
41. R. J. Ward, F. A. Zucca, J. H. Duyn, R. R. Crichton, L. Zecca, The role of iron in brain ageing and neurodegenerative disorders. *Lancet Neurol.* **13**, 1045–1060 (2014).
42. S. von Haehling, E. A. Jankowska, D. J. van Veldhuisen, P. Ponikowski, S. D. Anker, Iron deficiency and cardiovascular disease. *Nat. Rev. Cardiol.* **12**, 659–669 (2015).
43. J. A. Simcox, D. A. McClain, Iron and diabetes risk. *Cell Metab.* **17**, 329–341 (2013).
44. L. M. Coussens, Z. Werb, Inflammation and cancer. *Nature* **420**, 860–867 (2002).
45. N. Ruparelia, J. T. Chai, E. A. Fisher, R. P. Choudhury, Inflammatory processes in cardiovascular disease: A route to targeted therapies. *Nat. Rev. Cardiol.* **14**, 133–144 (2017).
46. D. Furman *et al.*, Chronic inflammation in the etiology of disease across the life span. *Nat. Med.* **25**, 1822–1832 (2019).
47. G. Toker, E. Küpeli, M. Memisoğlu, E. Yesilada, Flavonoids with antinociceptive and anti-inflammatory activities from the leaves of *Tilia argentea* (silver linden). *J. Ethnopharmacol.* **95**, 393–397 (2004).
48. C. Spagnuolo, S. Moccia, G. L. Russo, Anti-inflammatory effects of flavonoids in neurodegenerative disorders. *Eur. J. Med. Chem.* **153**, 105–115 (2018).
49. R. Y. Pan *et al.*, Sodium rutin ameliorates Alzheimer's disease-like pathology by enhancing microglial amyloid-β clearance. *Sci. Adv.* **5**, eaau6328 (2019).
50. P. Rockenfeller *et al.*, Diacylglycerol triggers Rim101 pathway-dependent necrosis in yeast: A model for lipotoxicity. *Cell Death Differ.* **25**, 767–783 (2018).
51. R. L. Minster *et al.*, A thrifty variant in CREBRF strongly influences body mass index in Samoans. *Nat. Genet.* **48**, 1049–1054 (2016).
52. S. Das *et al.*, An investigation into the identification of potential inhibitors of SARS-CoV-2 main protease using molecular docking study. *J. Biomol. Struct. Dyn.* **13**, 1–11 (2020).
53. A. G. Manzoni *et al.*, Hyperlipidemia-induced lipotoxicity and immune activation in rats are prevented by curcumin and rutin. *Int. Immunopharmacol.* **81**, 106217 (2020).
54. R. Khlifi *et al.*, *Erica multiflora* extract rich in quercetin-3-O-glucoside and kaempferol-3-O-glucoside alleviates high fat and fructose diet-induced fatty liver disease by modulating metabolic and inflammatory pathways in Wistar rats. *J. Nutr. Biochem.* **86**, 108490 (2020).
55. K. Zandi *et al.*, Antiviral activity of fisetin, rutin and naringenin against Dengue virus type-2. *J. Med. Plants Res.* **5**, 5534–5539 (2011).
56. L. Yarmolinsky, M. Huleihel, M. Zaccai, S. Ben-Shabat, Potent antiviral flavone glycosides from *Ficus benjamina* leaves. *Fitoterapia* **83**, 362–367 (2012).
57. S. J. Dixon *et al.*, Ferroptosis: An iron-dependent form of nonapoptotic cell death. *Cell* **149**, 1060–1072 (2012).
58. W. H. Xu, C. H. Li, T. L. Jiang, Ferroptosis pathway and its intervention regulated by Chinese materia medica. *Zhongguo Zhongyao Zazhi* **43**, 4019–4026 (2018).
59. H. E. Johnson, S. A. Banack, P. A. Cox, Variability in content of the anti-AIDS drug candidate prostratin in Samoan populations of *Homalanthus nutans*. *J. Nat. Prod.* **71**, 2041–2044 (2008).

10 of 11 | PNAS
https://doi.org/10.1073/pnas.2100880118

Molimau-Samasoni et al.
Functional genomics and metabolomics advance the ethnobotany of the Samoan traditional medicine "matalafi"

60. M. Chieppa, G. Giannelli, Immune cells and microbiota response to iron starvation. *Front. Med. (Lausanne)* **5**, 109 (2018).

61. P. A. Cox, Saving the ethnopharmacological heritage of Samoa. *J. Ethnopharmacol.* **38**, 181–188 (1993).

62. M. C. Leal *et al.*, Fifty years of capacity building in the search for new marine natural products. *Proc. Natl. Acad. Sci. U.S.A.* **117**, 24165–24172 (2020).

63. I. Vandebroek *et al.*, Reshaping the future of ethnobiology research after the COVID-19 pandemic. *Nat. Plants* **6**, 723–730 (2020).

64. D. G. Robinson *et al.*, Design and analysis of Bar-seq experiments. *G3: Genes/Genomes/Genet.* **4**, 11–18 (2014).

65. T. Zhang *et al.*, An improved method for whole protein extraction from yeast *Saccharomyces cerevisiae. Yeast* **28**, 795–798 (2011).

66. D. O'Sullivan *et al.*, Treatment with the antipsychotic agent, risperidone, reduces disease severity in experimental autoimmune encephalomyelitis. *PLoS One* **9**, e104430 (2014).

67. X. Zhang, R. Goncalves, D. M. Mosser, The isolation and characterization of murine macrophages. *Curr. Protoc. Immunol.* **83**, 14.1.1–14.1.14 (2008).

68. T. Pluskal, S. Castillo, A. Villar-Briones, M. Oresic, MZmine 2: Modular framework for processing, visualizing, and analyzing mass spectrometry-based molecular profile data. *BMC Bioinformatics* **11**, 395 (2010).

69. M. C. Chambers *et al.*, A cross-platform toolkit for mass spectrometry and proteomics. *Nat. Biotechnol.* **30**, 918–920 (2012).

70. P. Shannon *et al.*, Cytoscape: A software environment for integrated models of biomolecular interaction networks. *Genome Res.* **13**, 2498–2504 (2003).

PLANT BIOLOGY

SOCIAL SCIENCES

Molimau-Samasoni et al.
Functional genomics and metabolomics advance the ethnobotany of the Samoan traditional medicine "matalafi"

PNAS | **11 of 11**
https://doi.org/10.1073/pnas.2100880118